Introduction to Basic Concepts of Gravitational Lensing

Ramesh Narayan, Sylvanie Wallington

Harvard-Smithsonian Center for Astrophysics, 60 Garden Street, Cambridge, Massachusetts 02138 USA

1 Introduction

This article provides a brief introduction to the basic theoretical concepts used in the field of gravitational lensing. Since most of the ideas are well-known to those who are active in this field, no attempt is made to cite original references. For more details on individual issues, the reader is referred to the review articles by Blandford & Kochanek (1987a), Canizares (1987), Refsdal & Kayser (1988), Fort (1990), Surdej (1990), Blandford & Narayan (1992), and the forthcoming monograph by Schneider, Ehlers & Falco (1992).

2 Rays and Deflections

Figure 1 shows a light ray from a source S being deflected through an angle $\hat{\alpha}$ by a deflector or lens L and being received by an observer O at an angle θ with respect to some reference direction. The angular position of the image θ is related to the source's "true" position, β , by the following lens equation,

$$\overrightarrow{\beta} = \overrightarrow{\theta} - \overrightarrow{\alpha}(\overrightarrow{\theta}), \qquad \overrightarrow{\alpha}(\overrightarrow{\theta}) = \frac{D_{\rm ds}}{D_{\rm s}} \hat{\overrightarrow{\alpha}}(\overrightarrow{\xi}), \tag{1}$$

where ξ is the impact parameter of the ray at the lens and $D_{\rm ds}$, $D_{\rm s}$ are angular diameter distances. In general, the angles β , θ , α , and $\hat{\alpha}$ will not be coplanar. Therefore, (1) has been written in its vector form, where each angle has two components in the plane of the sky.

Under most circumstances, the line-of-sight thickness of the gravitational lens is much less than D_d , D_{ds} , or D_s . In this "thin lens" limit, the deflection

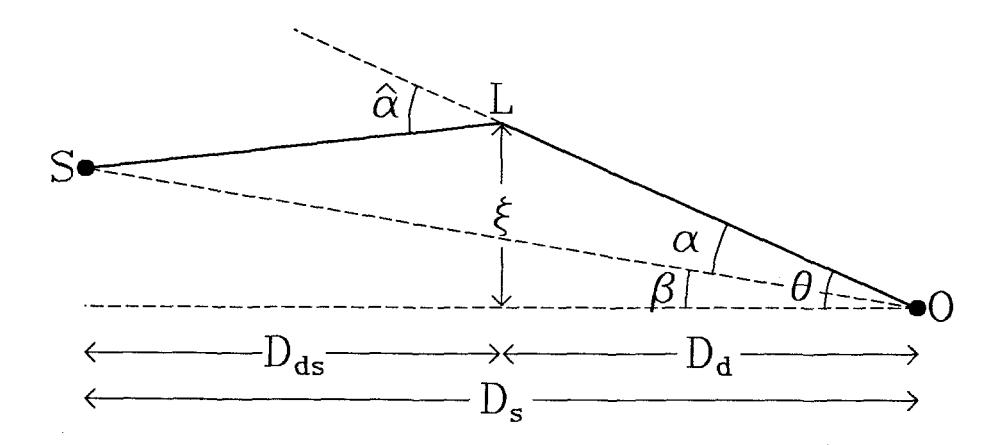


Fig. 1. Basic geometry of gravitational lensing. A light ray from a source S at redshift z_s is incident on a deflector or lens L at redshift z_d with impact parameter ξ relative to some lens "center". Assuming the lens is thin compared to the total path length, the deflection angle of the ray is $\hat{\alpha}(\xi)$ in crossing the lens plane. The deflected ray reaches the observer O, who sees the image of the source apparently at position θ on the sky. The true direction of the source, *i.e.* its position on the sky in the absence of the lens, is given by β . The angular diameter distances D_d , D_s , and D_{ds} separate the source, deflector, and observer.

angle $\overrightarrow{\alpha}$ depends only on the surface mass density of the lens $\Sigma(\overrightarrow{\xi})$, and is given by the two dimensional gradient of a potential $\psi(\overrightarrow{\xi})$,

$$\widehat{\overrightarrow{\alpha}}(\overrightarrow{\xi}) = \frac{1}{c^2} \overrightarrow{\nabla_{\xi}} \psi(\overrightarrow{\xi}), \text{ where } \nabla_{\xi}^2 \psi(\overrightarrow{\xi}) = 8\pi G \Sigma(\overrightarrow{\xi}).$$
 (2)

The Poisson equation on the right is in two dimensions and has an extra factor of 2 relative to Newtonian gravity. Equation (2) may be equivalently expressed through the Green's function of the Poisson operator, viz.

$$\hat{\overrightarrow{\alpha}}(\overrightarrow{\xi}) = \int \int d^2 \xi' \frac{4G\Sigma(\overrightarrow{\xi'})}{c^2} \frac{(\overrightarrow{\xi} - \overrightarrow{\xi'})}{|\overrightarrow{\xi} - \overrightarrow{\xi'}|^2}.$$
 (3)

In general, the ray path corresponding to an observed image of a lensed source has a *time delay* relative to the direct ray from the source to the observer in the absence of the lens. This delay is given by

$$t(\overrightarrow{\theta}) = \frac{(1+z_d)D}{2c} |\overrightarrow{\theta} - \overrightarrow{\beta}|^2 - \frac{(1+z_d)}{c^3} \psi(D_d \overrightarrow{\theta}), \tag{4}$$

where z_d is the redshift of the deflector and D is an effective distance defined by

$$D = \frac{D_{\rm d}D_{\rm s}}{D_{\rm ds}}. (5)$$

The relative time delay between two images, $t(\overrightarrow{\theta_i}) - t(\overrightarrow{\theta_j})$, is potentially measurable if the source has intrinsic variations.

3 Simple Lens Models

Using (2) or (3) the ray deflection angle $\overrightarrow{\alpha}(\overrightarrow{\xi})$ can be determined for any lens mass distribution, but this full generality is rarely employed. Instead, one often considers simple models for $\Sigma(\overrightarrow{\xi})$ [or $\psi(\overrightarrow{\xi})$] where the deflection law $\widehat{\alpha}(\overrightarrow{\xi})$ may be written down explicitly.

A particularly simple model is a mass sheet of constant density Σ . Here $\hat{\alpha} = (4\pi G \Sigma/c^2)\xi$ and the lens equation gives

$$\beta = \left(1 - \frac{\Sigma}{\Sigma_{\rm cr}}\right)\theta \equiv (1 - \kappa)\theta, \qquad \Sigma_{\rm cr} = \frac{c^2}{4\pi GD}.$$
 (6)

The convergence κ , which is proportional to Σ , describes the focusing power of the sheet. As (6) shows, a mass sheet behaves like a perfect magnifying lens, where the linear dimensions of a source are magnified by a factor of $(1-\kappa)^{-1}$, and because surface brightness is conserved, the net flux received from a source is magnified by $\mu = (1-\kappa)^{-2}$. Thus the magnification is infinite when Σ is equal to the *critical density* Σ_{cr} .

If, in addition to the convergence due to a mass sheet, there is also an external shear γ due to tidal effects of distant masses, then in the appropriate principal axes (6) becomes

$$\beta_{1,2} = (1 - \kappa \mp \gamma)\theta_{1,2},$$

$$[\mu] = \frac{\partial \overrightarrow{\theta}}{\partial \overrightarrow{\beta}} = \begin{bmatrix} (1 - \kappa - \gamma)^{-1} & 0\\ 0 & (1 - \kappa + \gamma)^{-1} \end{bmatrix}.$$
(7)

The magnification tensor $[\mu]$ is now anisotropic, but in general symmetric. The determinant of this matrix gives the flux magnification,

$$\mu = |[\mu]| = [(1 - \kappa)^2 - \gamma^2]^{-1}.$$
 (8)

The constant density sheet with shear is sometimes used to model large smoothly varying lens mass distributions, e.g. the cluster in Q0957+561 (cf Falco et al. 1991). However, the concepts introduced above have a wider validity. For instance, the local magnification tensor associated with a lensed quasar image can be decomposed into a convergence due to the local surface density of the lens and a shear from the mass in the rest of the lens. It can

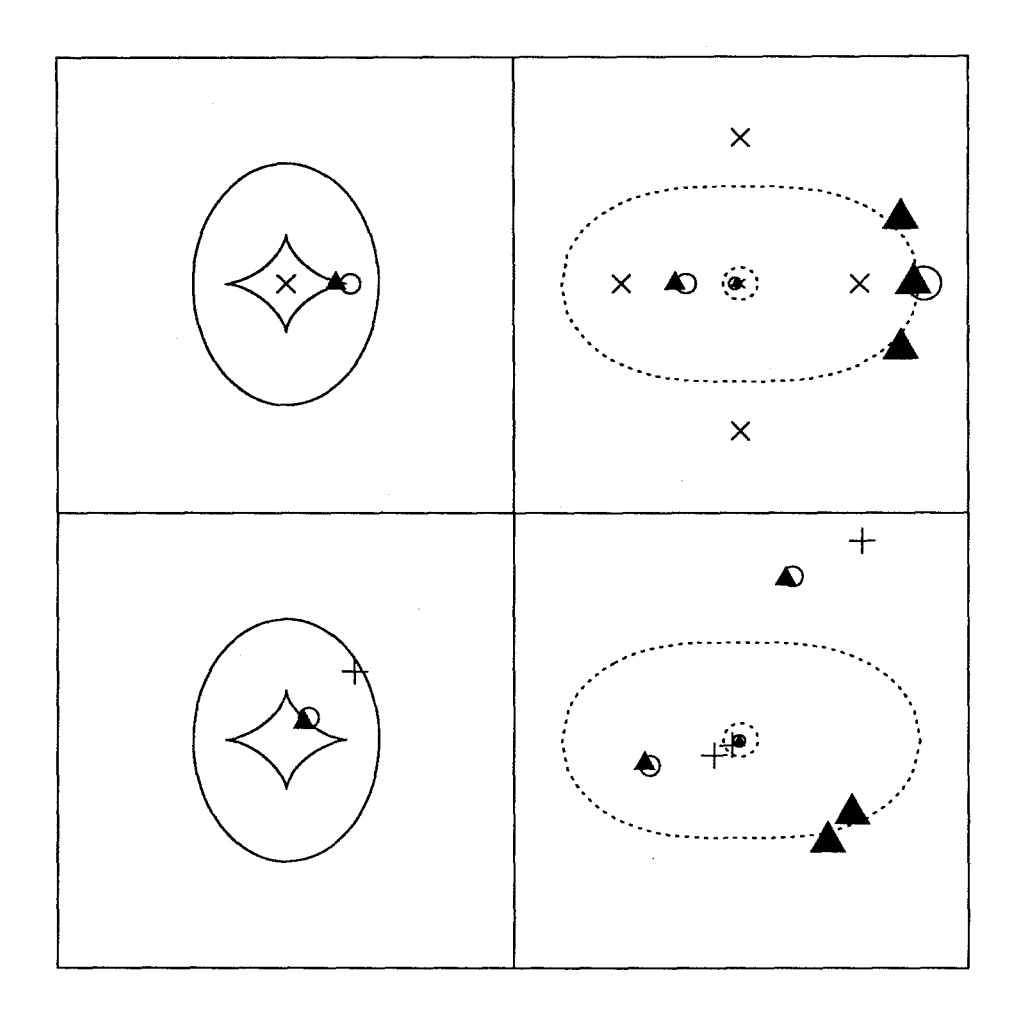


Fig. 2. Multiple imaging of point sources at fixed redshift by a generic elliptical lens. The solid lines in the left panels are caustics (cf sec. 5) that separate regions in the source plane corresponding to different image multiplicities (1, 3, or 5). The inner, or tangential caustic has four cusps connected by fold lines. The outer radial caustic is a pure fold. The outer dashed lines in the right panels are tangential critical curves and the inner ones are radial critical curves. Critical curves are the lines on which the two "extra" images merge and become infinitely magnified before disappearing as the source crosses a caustic. The symbols show representative source positions and the corresponding image locations. When the source is close to a caustic, some of the images are strongly magnified, indicated by large symbols in the image panels. One of the multiple images usually occurs near the center of the lens and is strongly demagnified if the core radius of the lens is small. This is indicated by a smaller symbol.

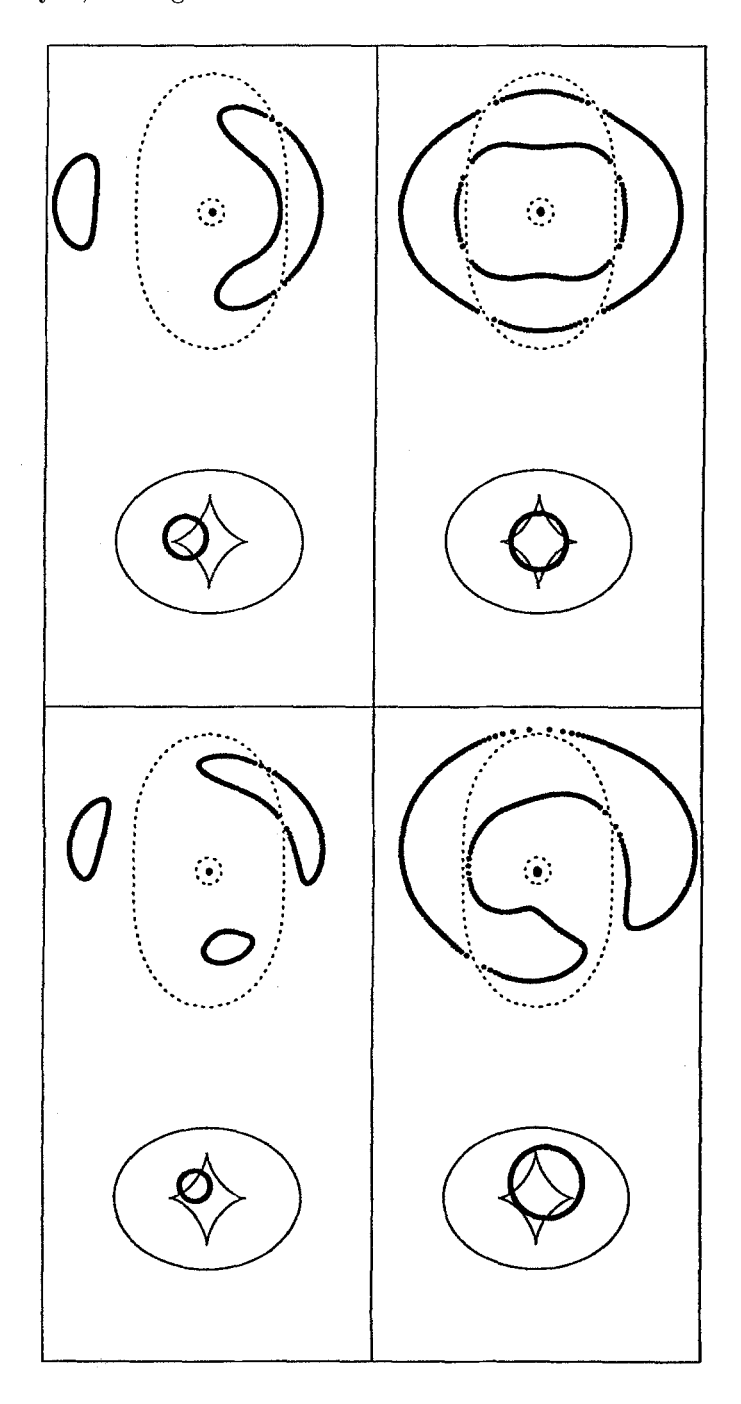


Fig. 3. Representative arc and ring images of resolved, extended sources produced by an elliptical lens. In each set, the source planes are on the left and the corresponding images are on the right.

also be shown that (barring some unusual exceptions), a lens can produce multiple images only if its surface density exceeds $\Sigma_{\rm cr}$ at some point.

Consider next a point lens of mass M. In this case $\hat{\alpha}(\xi) = 4GM/c^2\xi$, and it is convenient to define

$$\theta_E = \left(\frac{4GM}{c^2D}\right)^{1/2} \sim 1'' \left(\frac{M}{10^{11}M_{\odot}}\right)^{1/2} \left(\frac{D}{1\text{Gpc}}\right)^{-1/2}.$$
 (9)

The angle $\theta_{\rm E}$ is referred to as the *Einstein radius* of the lens. If a point source is aligned exactly with the lens, then its image will consist of a ring (an "Einstein ring") of radius $\theta_{\rm E}$. While such a ring image of a point source requires an extraordinary alignment and is quite unlikely to occur in practice, $\theta_{\rm E}$ is nevertheless a useful quantity to characterize the properties of the lens. If the source position β (measured with respect to the position of the lens) is $\lesssim \theta_{\rm E}$, then two comparably bright images of the source are produced, with an angular separation $\sim 2\theta_{\rm E}$. Equation (9) then shows that galaxy lenses ($M \sim 10^{11} M_{\odot}$) will produce multiple images with angular separations ~ 1 ", while galaxy clusters ($M \gtrsim 10^{14} M_{\odot}$) will produce separations ~ 1 ". If $\beta \gg \theta_{\rm E}$, there will be a primary image of the source that is hardly perturbed (either in position or intensity), and a secondary image located close to the point lens and demagnified by a factor $\sim (\theta_{\rm E}/\beta)^4$.

For modeling galaxy lenses, a somewhat better model than the point lens is the *singular isothermal sphere* of one dimensional velocity dispersion σ . For such a lens,

$$\hat{\alpha}(\xi) = 4\pi \frac{\sigma^2}{c^2},$$

$$\theta_{\rm E} = 4\pi \frac{\sigma^2}{c^2} \frac{D_{\rm ds}}{D_{\rm s}} \sim 1'' \left(\frac{\sigma}{250 \text{ km s}^{-1}}\right)^2.$$
(10)

Here multiple imaging is possible if $\beta < \theta_{\rm E}$, in which case there are two images, one at $\beta + \theta_{\rm E}$ and the other at $\beta - \theta_{\rm E}$. A third image is technically present at $\theta = 0$, but it is infinitely demagnified. The singularity at the origin can be removed by giving the mass distribution a core radius ξ_c such that, for $\xi < \xi_c$, $\Sigma(\xi)$ deviates from its isothermal $1/\xi$ behavior and tends instead to a constant. In this model, multiple imaging is possible only if $\Sigma(0) > \Sigma_{\rm cr}$, which requires $\xi_c \lesssim D_{\rm d}\theta_{\rm E}$. If this condition is satisfied and if $\beta \lesssim \theta_{\rm E}$, then there are three images: two located approximately at $\sim \beta \pm \theta_{\rm E}$ and a third superimposed on the lens core with a magnification $\sim (\xi_c/D_{\rm d}\theta_{\rm E})^2$.

The total cross-section for multiple imaging by a gravitational lens can be defined as the angular area within which the source must be located in order to be multiply imaged. In the case of the singular isothermal sphere the cross-section is exactly $\pi\theta_{\rm E}^2$, while for the non-singular case it is less.

The singular and non-singular isothermal spheres are convenient models that are useful for approximate order-of-magnitude estimates of certain lensing properties. However, they suffer from being too symmetric and consequently being unable to explain many of the observed cases of lensing. For instance, they cannot produce four images, as seen often in multiply-imaged quasars, or single giant arcs, as seen in cluster lensing. It turns out that by breaking the circular symmetry of the lens and introducing a quadrupolar distortion, the qualitative features of almost all the observed lenses can be reproduced. Such a model is referred to as an *elliptical lens*. The particular manner in which the quadrupole term is introduced does not appear to be important. The following bending law (Blandford & Kochanek 1987b), which corresponds to a simple generalization of the non-singular isothermal sphere, is a convenient model of an elliptical lens,

$$\hat{\alpha}_{1,2}(\xi_1, \xi_2) = 4\pi \frac{\sigma^2}{c^2} \frac{(1 \mp \epsilon)\xi_{1,2}}{[\xi_c^2 + (1 - \epsilon)\xi_1^2 + (1 + \epsilon)\xi_2^2]^{1/2}}.$$
 (11)

The subscripts 1, 2 refer to components along the two principal axes of the lens and ϵ measures the "ellipticity" of the lens.

Figures 2 and 3 give an idea of the variety of image configurations possible with an elliptical lens. Figure 2 shows some possible configurations for multiple imaging of point sources, and Figure 3 shows various results of lensing extended sources. A comparison with the observed examples of lensing shows that all of the observed morphologies seen in multiply-imaged quasars, luminous arcs, and radio rings arise naturally in an elliptical lens.

4 Fitting a Lens Model to Observations

A successful model of a multiply-imaged quasar must fit the positions $\overrightarrow{\theta_i}$ of each of the n images of a source using the same source position $\overrightarrow{\beta}$. Since $\overrightarrow{\beta}$ itself is unknown, this gives 2(n-1) constraints. If the images are resolved, each image pair provides a relative magnification tensor $[\mu_{ij}] = [\mu_i][\mu_i]^{-1}$. This leads to 4(n-1) constraints. In the case of Q0957+561 (where n=2), four constraints have been obtained from VLBI observations (Falco et al. 1991). More generally, only flux ratios $\mu_{ij} = |[\mu_{ij}]|$ are measured; these provide (n-1) constraints. If relative time delays between the images are measured, e.g. Q0957+561 (Lehar et al. 1992, Press et al. 1992), then one can have up to (n-1) additional constraints. All of these constraints may be used to fit a parameterized model of the lens. Some of the parameters may also be determined through direct observations of the lens, e.g. the velocity dispersion σ in Q0957+561 (Rhee 1991) and the surface brightness distribution in Q2237+0305 (Schneider et al. 1988). Successful models have been developed for all the well-observed multiple quasars including the problematical Q2016+112 (though the model proposed by Narasimha et al. 1987 for this object seems a little contrived).

In the case of resolved sources, a different strategy is employed. Since surface brightness is preserved in gravitational lensing, for each position $\overrightarrow{\beta}$ in the source there are constraint equations of the form

$$I(\overrightarrow{\theta^{(1)}}) = I(\overrightarrow{\theta^{(2)}}) = \dots = I(\overrightarrow{\theta^{(n)}}) = I_s(\overrightarrow{\beta}),$$
 (12)

where $I_s(\overrightarrow{\beta})$ is the surface brightness of the source at position $\overrightarrow{\beta}$ and $I(\overrightarrow{\theta^{(i)}})$ is the observed surface brightness at the position of its *i*'th image. With well-resolved sources, one can thus obtain many more constraints than with multiply-imaged point sources. Indeed, with data at multiple wavelengths/colors and with polarization, lens models should be quite well-constrained. Kochanek *et al.* (1989) have developed a successful model for the radio ring MG1131+0456 using this method.

5 Caustics

The lines in the source plane that separate regions of different image multiplicity are referred to as caustics. In Figs. 2 and 3, there are two caustics separating the 1-, 3- and 5-image regions. The generic caustics in the two-dimensional $\overrightarrow{\beta}$ plane are the fold (which has the topology of a line) and the cusp (which is a singular point connecting two folds). An elliptical lens has either two or four cusps. If the three-dimensional source space is considered, where the third dimension is the source redshift, then folds occur in sheets, cusps occur in lines, and higher-order caustics like swallowtails and umbilics could be present at isolated points.

Caustics are important because sources that are located in their vicinity are highly magnified. If a source is located at a small angular distance $\Delta\beta$ from a fold caustic on the higher multiplicity side, the two extra images will generically have magnifications that scale as $\mu \propto \Delta\beta^{-1/2}$ (e.g. Blandford & Narayan 1986). Thus the magnification diverges as $\Delta\beta \to 0$. However, the two infinitely bright images vanish completely when the source crosses the fold, producing a discontinuous change in μ .

Let us define $\sigma(>\mu)$ as the cross-section in the β plane corresponding to magnifications greater than μ . It is straight-forward to show that the high magnifications associated with a fold give a scaling $\sigma(>\mu) \propto \mu^{-2}$ or $d\sigma/d\mu \propto \mu^{-3}$, for large μ . This result has been extensively used in theories of microlensing and in discussions of magnification bias (see below).

In the case of a cusp three images are involved. For a source just inside the cusp there are three highly brightened images, while if the source is just outside there is a single brightened image. A crucial feature that distinguishes the cusp from the fold is that even the lower multiplicity region can have very large magnifications. The cross-section here scales as

 $\sigma(>\mu) \propto \mu^{-5/2}$ or $d\sigma/d\mu \propto \mu^{-7/2}$ for large μ , which is steeper than the scaling due to a fold.

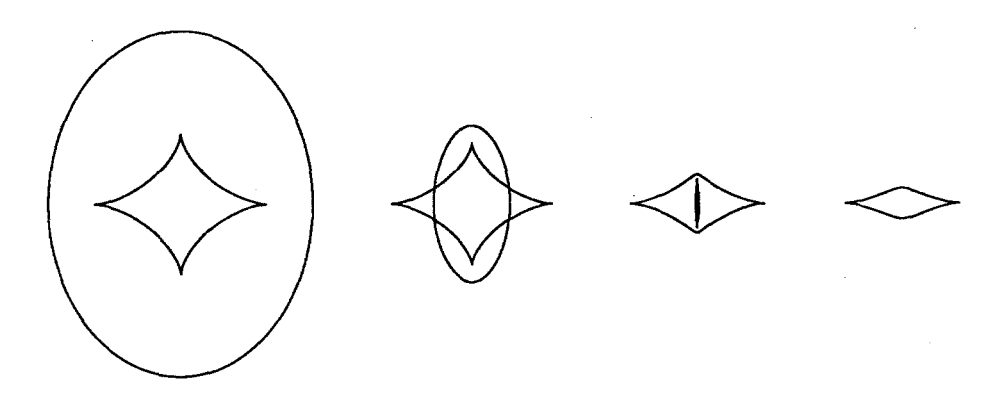


Fig. 4. The evolution of the caustic structure with increasing core radius. Core radius ξ_c increases from left to right in this diagram, and has values of $\xi_c/D_d\theta_E = 0.05, 0.4, 0.75$, and 0.9 respectively. In each of the first three diagrams the most central region is the area which produces 5 images, the area outside of all caustics produces 1 image, and the intermediate areas produce 3. In the fourth configuration the regions inside and outside the caustic produce 3 images and 1 image respectively. Not shown here is a final transition at $\xi_c/D_d\theta_E = 1 + \epsilon$ when the remaining double-cusped caustic shrinks to nothing and all source positions have only one image.

The caustic configuration for elliptical lenses varies with the core radius of the lens. Figure 4 shows the progression as a function of increasing core radius in an $\epsilon = 0.2$ lens. At small angular core radii, i.e. $\xi_c/D_d \ll \theta_E$, there is a four-cusped inner caustic which is wholly contained within an outer fold. (This is the case shown in Figs. 2 and 3 and corresponds to a normal galaxy lens with a linear core radius $\xi_c \lesssim 0.5$ kpc at a cosmological distance.) As the angular core radius increases, the inner caustic breaks through the outer caustic, and the outer caustic shrinks. The two caustics eventually penetrate each other (through a hyperbolic umbilic caustic), and separate again, leaving two nested lips caustics, each with two cusps. The inner lips caustic then continues to shrink until at $\xi_c/D_d = (1 - \epsilon)\theta_E$ it disappears altogether, leaving only a single lips caustic with 1- and 3-image regions. The remaining caustic, too, continues to shrink and finally disappears when $\xi_c/D_d = (1+\epsilon)\theta_E$. Beyond this core radius there can be no multiple imaging.

Clusters of galaxies tend to have values of $\xi_c/D_d\theta_E \sim 1$, and so the later examples in the sequence shown in Fig. 4 are relevant for modeling them. They are also needed for galaxy lenses that are close to either the source or the observer. A feature of these caustic configurations is that they have exposed cusps that directly adjoin the single image region of the source

plane. Sources located on or close to such cusps make large arcs without counter-images (Fig. 5). The majority of luminous arcs observed in clusters do not have counter-images, as one might expect on the basis of their large core radii. See the article by Kochanek in this volume for a more detailed discussion of caustics and arcs.

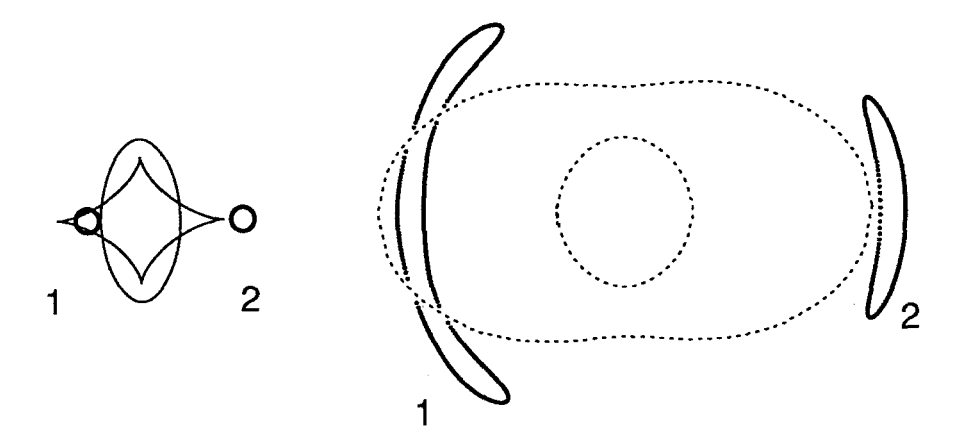


Fig. 5. Arc images of extended sources produced by a $\xi_c = 0.4$ elliptical lens. Here we have two exposed cusps that directly adjoin the single-image region, in contrast to the case shown in Fig. 3 where all the cusps are in the interior. When an extended source is located on an exposed cusp, a large arc image is produced without any counter-image. Even when the source is slightly off the caustic, a moderately elongated image is still possible because of the tangential stretching introduced by the nearby cusp.

6 Magnification Bias, Lensing Probabilities

Caustics and their scalings are particularly important for the phenomenon of magnification bias. For simplicity, consider first a population of sources at a fixed redshift, and a set of $n_{\rm L}$ foreground lenses. Let each lens have a cross-section for multiple images described by $\sigma(>\mu)$ (steradians). The probability that a given source will be multiply imaged is then

$$p = \frac{n_{\rm L}}{4\pi}\sigma(>1). \tag{13}$$

(We have used the fact that multiple-imaging is always accompanied by a net magnification $\mu > 1$.) Suppose the sources have a range of intrinsic luminosities described by the number counts $N_{\rm Q}(< m)$ which gives the number of sources with apparent magnitude brighter than m. When a source is lensed, its apparent magnitude is modified to $m - 2.5 \log \mu$. Hence, the

number of lensed sources $N_{\rm LQ}(< m)$ expected to be discovered in a fluxlimited survey is

$$N_{\rm LQ}(< m) = pN_{\rm Q}(< m) + \frac{n_{\rm L}}{4\pi} \int_{m}^{\infty} \sigma[> 10^{0.4(m'-m)}] \frac{dN_{\rm Q}(< m')}{dm'} dm'.$$
 (14)

Equations (13) and (14) are both easily generalized to include a range of source and lens redshifts. Equation (14) consists of two parts: (i) a straightforward estimate, $pN_{\mathbf{Q}}(< m)$, which is the product of the number of sources and the probability of lensing, plus (ii) an additional contribution from sources that are intrinsically fainter than the magnitude cut-off but that are magnified above the limit by lensing. The occurrence of an excess of lensed sources in flux-limited samples, over and above the naive estimate given by the first term, is referred to as magnification bias (Turner *et al.* 1984). Since the bias is a consequence of high magnifications, it is strongly influenced by the properties of the caustics. Magnification bias is quantified by the following bias factor,

$$B(< m) = \frac{N_{LQ}(< m)}{pN_{Q}(< m)}.$$
 (15)

This factor can be quite large if the intrinsic counts $N_{\mathbf{Q}}(< m)$ are sufficiently steep.

Figures 6 and 7 show the results of model calculations we have carried out for a population of elliptical lenses described by the deflection law given in (11). The lenses were assumed to have ellipticity $\epsilon = 0.2$, a Schechter luminosity function appropriate for galaxies, and velocity dispersions following the Faber-Jackson relation, $L \propto \sigma^4$. The core radius ξ_c was assumed to scale as σ^2 , with $\xi_c = 100$ pc for an L^* galaxy with $\sigma = 220$ km s⁻¹. The number density of galaxies was selected such that the parameter F defined by Turner et al. (1984),

$$F \equiv \frac{16\pi^3}{cH_o^3} \langle n_{\rm L} \sigma^4 \rangle, \tag{16}$$

has a value of F = 0.025. This is approximately a factor of 2 lower than the value used by Fukugita & Turner (1991) and Kochanek (1991).

The dashed line in Fig. 6 shows the cumulative number counts of quasars as computed using model B of Boyle et al. (1988) for the quasar luminosity function. The slope of this curve is 0.18 for $m_{\rm B}>19$ and 1.12 for bright magnitudes, corresponding to power-law indices of -0.44 and -2.79 respectively when expressed in terms of luminosity rather than magnitude. (Equivalently, the slopes of the differential luminosity function $d\phi/dL$ are -1.44 and -3.79.) The solid lines labeled 3 and 5 show the calculated number counts of multiply-imaged quasars with 3 and 5 images respectively. The line labeled 1 refers to sources that are not multiply-imaged but magnified

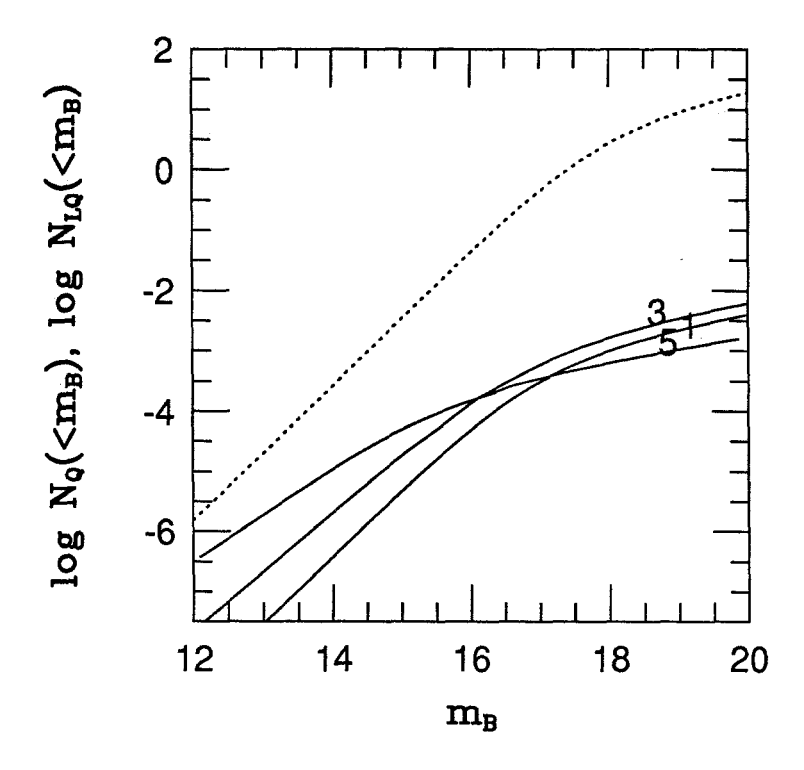


Fig. 6. Cumulative number counts of lensed and unlensed quasars. The dotted line shows the number of quasars per square arcsecond of the sky brighter than a given magnitude, m_B . The solid lines give the predicted numbers of lensed quasars broken down by image multiplicity. Notice the different slopes of the solid curves at bright magnitudes due to differences in the influence of caustics on the 1-, 3-, and 5-image regions of the source plane.

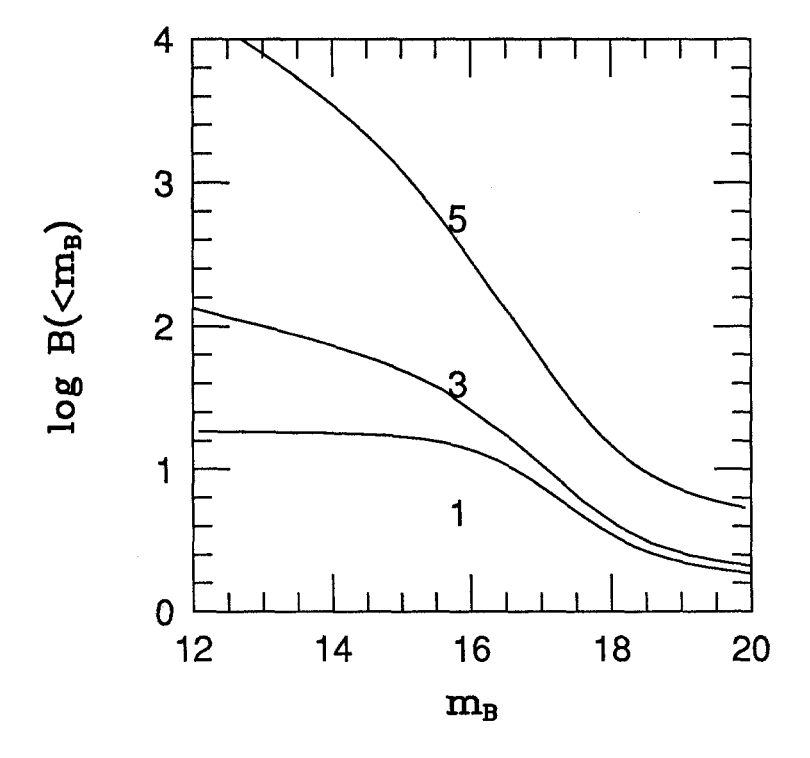


Fig. 7. The magnification bias factor B(< m) due to an elliptical lens. This quantity describes the tendency to overcount lensed sources in a magnitude limited survey. The effect arises because lensing brightens intrinsically fainter objects past the magnitude cut-off. Five image cases have particularly high bias at bright magnitudes. Even at faint magnitudes, they are overrepresented by a factor of 5.

by more than a factor of 2. These results are similar to those obtained by Kochanek (1991).

In this model, the intrinsic probability p (cf (13)) associated with the three cases of lensing are $p_1 = 6.0 \times 10^{-4}$, $p_3 = 1.1 \times 10^{-4}$, $p_5 = 1.2 \times 10^{-5}$. The actual fractions of lens candidates predicted in a flux-limited sample

are, however, significantly greater than this, particularly at bright magnitudes. This is because of magnification bias as indicated by the plots of the respective bias factors in Fig. 7. Note the extraordinary bias at bright magnitudes, particularly for 5 image cases. The most reliable optically selected lensed quasars all have $m \lesssim 17$, which makes them unusually bright. This is doubtless largely a consequence of magnification bias. Note also that although $p_5 \sim 0.1 p_3$, we still expect to find as many 5 image as 3 image lensed quasars at $m_{\rm B} \sim 16.5$. This is roughly in agreement with the observations.

An interesting point to note in Fig. 6 is that the three solid curves have different slopes at bright magnitudes. The 5 image statistics are dominated by fold-caustics and hence have a slope of 0.8, whereas the 3 image lenses in this case happen to be dominated by the exteriors of cusps and so have a slope of 1.0 (power-law indices of -2 and -5/2). The brightened single image quasars are not dominated by caustics and have the same slope as the intrinsic counts.

One final point of interest is that none of the observed cases of lensing (except the puzzling Q2016+112) have 3 or 5 images. Instead, in every case, we see either 2 or 4 images. Observational limits indicate the odd image is typically at least 10 to 100 times fainter than the observed bright images. One explanation for the missing images is that the lenses may have small core radii. Using the above model, we find that the core radius of an L^* galaxy must be $\xi_c \lesssim 200$ pc in order to explain the universal absence of the central image. This limit is consistent with recent high resolution observations of the cores of nearby galaxies (Lauer et al. 1991). It is, however, in conflict with lower limits, $\xi_c \gtrsim 1$ kpc, obtained by Narayan & Schneider (1990) for foreground galaxies in front of the BL Lac objects AO 0235+164 and PKS 0537-441.

This work was supported by the National Science Foundation under grant AST-9109525.

References

Blandford, R. D. & Kochanek, C. S. 1987a Dark Matter in the Universe, ed. J. Bahcall, T. Piran & S. Weinberg. Berlin: Springer-Verlag, p133

Blandford, R. D. & Kochanek, C. S. 1987b Ap. J. 321 658

Blandford R. D. & Narayan R. 1986 Ap. J. 310 568

Blandford, R. D. & Narayan, R. 1992 Annu. Rev. Astron. Astrophys. In press

Boyle, B. J., Shanks, T. & Peterson, B. A. 1988 MNRAS 235 935

Canizares, C. R. 1987 Observational Cosmology. Proc. IAU Symposium No. 124, ed. A. Hewitt, G. R. Burbidge & L.-Z. Fang. Dordrecht: Reidel, p729

Falco, E. E., Gorenstein, M. V. & Shapiro, I. I. 1991 Ap. J. 372 364

Fort, B. 1990 Gravitational Lensing, ed. Y. Mellier, B. Fort, and G. Soucail. Berlin: Springer-Verlag, p221

Fukugita, M. & Turner, E. L. 1991 MNRAS In press

Kochanek, C. S. 1991 Ap. J. 379 517

Kochanek, C. S., Blandford, R. D., Lawrence, C. R. & Narayan, R. 1989 MNRAS 238 43

Lauer, T. R. et al. 1991 Ap. J. Lett. 369 L41

Lehar, J., Hewitt, J. N., Roberts, D. H. & Burke, B. F. 1992 Ap. J. In press

Narasimha, D., Subramanian, K. & Chitre, S. M. 1987 Ap. J. 315 434

Narayan, R. & Schneider, P. 1990 MNRAS 243 192

Press, W. H., Rybicki, G. B. & Hewitt, J. N. 1992 Ap. J. In press

Refsdal, S. & Kayser, R. 1988 The Post-Recombination Universe, ed. N. Kaiser & A. Lasenby. Dordrecht: Kluwer, p297

Rhee, G. 1991 Nature 350 211

Schneider, D. P., Turner, E. L., Gunn, J. E., Hewitt, J. N., Schmidt M. & Lawrence, C. R. 1988 Astronom. J. 95 1619

Schneider, P., Ehlers, J. & Falco, E. E. 1992 Gravitational Lensing. Berlin: Springer-Verlag, In press

Surdej, J. 1990 Gravitational Lensing, ed. Y. Mellier, B. Fort, and G. Soucail. Berlin: Springer-Verlag, p57

Turner, E. L., Ostriker, J. P. & Gott, J. R. 1984 Ap. J. 284 1